Inorg. Chem. **2006**, *45*, 9818–9825

Pressure-Induced Internal Redox Reaction of $Cs_2[PdI_4]\cdot I_2$, $Cs_2[PdBr_4]\cdot I_2$, and $Cs_2[PdCl_4]\cdot I_2$

Peter Heines,[†] Hans-Lothar Keller,*[,†] Marc Armbrüster,[‡] Ulrich Schwarz,[‡] and John Tse[§]

Anorganische Chemie, Universität Dortmund, Otto-Hahn-Strasse 6, D-44221 Dortmund, Germany, Max-Planck-Institut für Chemische Physik fester Stoffe, Nöthnitzer Strasse 40, D-01187 Dresden, Germany, and National Research Council, Steacie Institute for Molecular Science, 100 Sussex Drive, Ottawa, Ontario K1A 0R6, Canada

Received February 3, 2006

The pressure-induced redox reaction within the system $Cs_2[Pd^{2+}I_4]\cdot I_2/Cs_2[Pd^{4+}I_6]$ was investigated by means of powder X-ray diffraction. Analogous high-pressure X-ray diffraction experiments were performed on the isostructural compounds $Cs_2[PdX_4]\cdot I_2$ (X = Cl, Br). Additionally, the phase transition of $Cs_2[PdBr_4]\cdot I_2$ to $Cs_2[PdBr_4I_2]$ was characterized by means of Raman scattering experiments as well as theoretical calculations based on density functional theory. On the basis of experimentally determined crystal structure data, a pathway for the topology of the redox reactions was developed and outlined.

1. Introduction

Tetragonal mixed-valence gold compounds of the distorted perovskite type ($Cs_2Au^+Au^{3+}X_6$; X = I, Br, Cl)[1] exhibit pressure-induced gold valence transitions of the Au^+ and Au^{3+} states to Au^{2+}, which are associated with a structural phase transition from a tetragonally distorted perovskite to the cubic aristotype. The crystal structure at ambient pressure contains alternating linear $[Au^+X_2]^-$ and square planar $[Au^{3+}X_4]^-$ complexes forming a three-dimensional network consisting of vertex-sharing elongated $[Au^{3+}X_{6/2}]$ octahedra and compressed $[Au^+X_{6/2}]^{2-}$ octahedra (Figure 1). For the chloride, the gold positions become crystallographically equivalent at 52 kbar and electrons are transferred from Au^+ to Au^{3+} mediated by bridging chlorine atoms: the oxidation state of gold is assigned as Au^{2+}.[2]

Similarly, the system $Cs_2[PdI_4]\cdot I_2/Cs_2[PdI_6]$ shows an irreversible pressure-induced solid-state redox reaction.[3] When exposed to elevated pressures, the crystal structure changes symmetry from a defect perovskite $Cs_2[PdI_4]\cdot I_2$ (space group *I*4/*mmm*; Figure 2a) via an intermediate orthorhombic phase (space group *Immm*) to the cubic arrangement $Cs_2[PdI_6]$ ($Fm\bar{3}m$; Figure 2b). In this process, Pd^{2+} is oxidized to Pd^{4+}. In $Cs_2[PdI_4]\cdot I_2$, the Pd^{2+} centers form four bonds to equidistant iodide ions, resulting in square-planar units. The palladium coordination is completed by iodine dumbbells oriented perpendicular to the $[PdI_4]$ units, thus constituting an elongated octahedron (Figure 2a). Above the transition pressure, all Pd−I distances become equal and regular octahedra are formed. The iodine molecule is cleaved and electrons are transferred from $[Pd^{2+}I_4]^{2-}$ units to I^0_2, resulting in $[Pd^{4+}I_6]^{2-}$ units. This process is supposed to be a direct electron transfer from palladium toward iodine, in contrast to $Cs_2Au^+Au^{3+}X_6$ (X = I, Br, Cl), where the electron transfer is mediated by bridging halogen atoms.

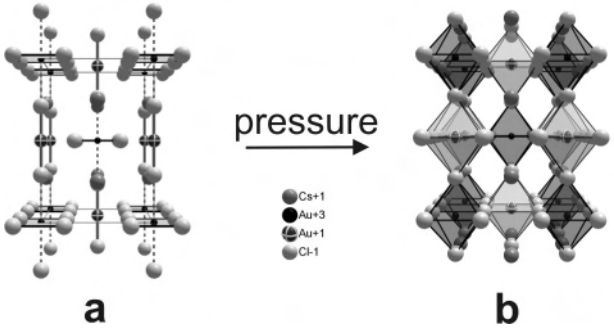

Figure 1. (a) Crystal structure of $Cs_2[Au^{3+}Cl_4][Au^+Cl_2]$. (b) Crystal structure of $Cs[Au^{2+}Cl_3]$ (tetragonal setting to highlight the structural change).

* To whom correspondence should be addressed. E-mail: hans-lothar.keller@uni-dortmund.de. Tel: +49 231 755 3804. Fax: +49 231 755 5048.
[†] Universität Dortmund.
[‡] Max-Planck-Institut für Chemische Physik fester Stoffe.
[§] National Research Council, Steacie Institute for Molecular Science.

(1) Kojima, N.; Matsushiuta, N. *Coord. Chem. Rev.* **2000**, *198*, 251−263.
(2) Denner, W.; Schulz, H.; D'Amour, H. *Acta Crystallogr.* **1979**, *A35*, 260−264.
(3) Schüpp, B.; Heines, P.; Keller, H.-L.; Savin, A. *Inorg. Chem.* **2000**, *39*, 732−735.

10.1021/ic0601945 CCC: $33.50
Published on Web 10/28/2006

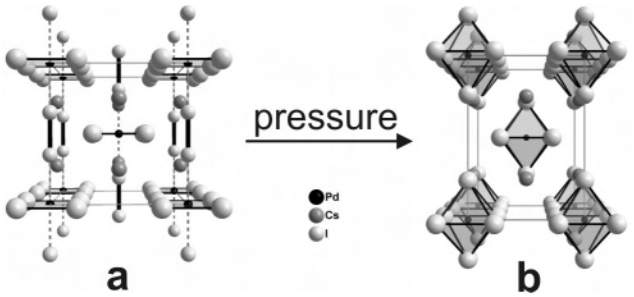

Figure 2. (a) Crystal structure of tetragonal $Cs_2[PdI_4]\cdot I_2$ (*I*4/*mmm*), a defect perovskite with a cation vacancy at (0, 0, $^1/_2$), coinciding with an elongation of the *c* axis. (b) Crystal structure of $Cs_2[PdI_6]$ in a tetragonal setting to highlight and visualize the structural changes.

To gain a more detailed insight into the structural changes associated with the reaction, we performed high-pressure X-ray diffraction experiments. Aiming to characterize local coordination changes, supplementary high-pressure Raman experiments were performed. Parallel, structural, and electronic changes were calculated by means of density functional theory (DFT) using the VASP computer program.[4] Here, we report an investigation concerning the phase transitions of the compounds $Cs_2[PdX_4]\cdot I_2$ (X = I, Br, Cl) at high pressures.

2. Experimental Section

Dark-red crystals of $Cs_2[PdI_4]\cdot I_2$ were prepared by solvothermal reaction of CsI, PdI_2, and I_2 (molar ratio 3:1:1) with 0.5 mL of freshly distilled hydroiodic acid (5.7% HI, bp 400.7 K) in closed quartz glass ampules at 450 K. Crystals of $Cs_2[PdBr_4]\cdot I_2$ and $Cs_2[PdCl_4]\cdot I_2$ were prepared by analogous reactions using CsX, PdX_2, and I_2 (2:1:1) in 0.5 mL of 4.7% (X = Br) and 3.2% (X = Cl) HX solutions. The products were washed with the diluted acids and diethyl ether. The purified products are monophasic, as determined by powder X-ray diffraction measurements. High-pressure X-ray diffraction experiments were performed at the ESRF (Grenoble, France) using stations ID09 and ID30. The stations are operated in transmission geometry with wavelengths of $\lambda = 0.415\ 86$ Å (ID09) and $\lambda = 0.373\ 80$ Å (ID30). Pressures for X-ray diffraction were generated by membrane-driven diamond-anvil cells[5] equipped with 300-μm diamond culets. Argon (ID09) and nitrogen (ID30) were used as pressure-transmitting media. Inconel gaskets (200-μm thickness) were preindented down to 60−80 μm before centric holes of 120 μm in diameter were generated by spark erosion. Thoroughly powdered samples were loaded into the cavities together with the liquid pressure-transmitting medium and a small ruby chip (ID30) or a samarium-doped strontium borate crystal (ID09) as the pressure sensor. Pressures were determined by the ruby luminescence method[6] using the calibration scale of Mao et al.[7] (ID30) or the method described by Datchi et al.[8] (ID09). Images of the powder diffraction rings were collected using an image-plate detector (mar345, diameter 345 mm, pixel size 100 μm × 100 μm) placed at a distance of approximately 400 mm (ID09) and 420 mm (ID30) to the sample, respectively. The aperture of the high-pressure cell was restricted to 25° in 2θ, giving a resolution of ~1 Å. By oscillation of the cell ±3° (ID09) or by horizontal/vertical movement of 10−15 μm in the *x* and *y* directions perpendicular to the beam (ID30), the so-called powder average was enhanced. The images were corrected for spatial distortion, nonlinear background features, saturated pixels, Lorentz factors, and polarization, before azimuthally integrating the diffraction rings using the software FIT2D.[9] Indexing was performed using the program DICVOL91.[10] Extraction of the intensities including the allocation of atoms within the unit cell was accomplished with the software EXPO.[11] Rietveld refinements of the collected high-pressure data were performed by applying the GSAS software suite.[12]

Raman spectra were recorded with a single grating spectrometer (LabRam System 010, Jobin Yvon) in backscattering geometry. For excitation, the 633-nm line of a He−Ne laser was used (laser power = 15 mW). The spectrometer was equipped with additional filters for low-frequency performance and a confocal microscope (objectives 20−100×). To probe for vibration selection rules, single crystals were oriented, a $\lambda/2$ plate was used to polarize the incident beam, and an analyzer was placed in the optical path behind the sample. To avoid decomposition of the samples, the laser power was reduced to 0.15 mW. Polarized single-crystal measurements were performed at ambient conditions with crystals fixed to glass capillaries mounted on a goniometer head. The crystals were oriented using X-ray diffraction techniques (Weissenberg and Laue) with a deviation of less than 0.3° along each crystallographic axis. The orientation of the *k* vector with respect to the crystallographic axes and the polarization of incident and scattered light for each experiment are given in Proto et al.'s notation.[13] In the experiments, the *x*, *y*, and *z* directions were parallel to the crystallographic *a*, *b*, and *c* axes, respectively. To ensure that observations are based on the Raman effect, Stokes and anti-Stokes modes were recorded. For the unpolarized high-pressure measurements, a fine powder of $Cs_2[PdBr_4]\cdot I_2$ was placed in a steel gasket in a diamond-anvil cell, which was equipped with type IIa diamonds. Paraffin was used as the pressure-transmitting medium and the ruby scale[7] for pressure calibration. Above 70 kbar, compressive stresses amount up to 2.5 kbar because of deviation from hydrostatic compression.[14] A total number of 18 spectra were recorded at pressures up to 106 kbar.

DFT calculations based on pseudopotential plane-wave methods[15] were performed in order to verify the crystal structures and electronic effects involved in the pressure-induced transformations of $Cs_2[PdBr_4]\cdot I_2$ to $Cs_2[PdBr_4I_2]$. All calculations involved the usage of the VASP package[4] and projected plane-wave (PAW) pseudopotentials[16] constructed of Perdew−Burke−Enzerhof functionals.[17] The PAW pseudopotentials, which imply the effects of core

(4) Kresse, G.; Furthmüller, J. *Phys. Rev.* **1996**, *B54*, 11169−11186; *Comput. Mater. Sci.* **1996**, *6*, 15−50.
(5) Le Toullec, R.; Princeaux, J. P.; Loubeyre, P. *High Pressure Res.* **1988**, *1*, 77−90.
(6) Piermarini, G. J.; Block, S.; Barnett, J. D.; Forman, R. A. *J. Appl. Phys.* **1975**, *46*, 2774−2780.
(7) Mao, H. K.; Xu, J.; Bell, P. M. *J. Geophys. Res.* **1986**, *B91*, 4673−4676.
(8) Datchi, F.; Le Toullec, R.; Loubeyre, P. *J. Appl. Phys.* **1987**, *81*, 3333−3339.
(9) Hammersley, A.; Svenson, S. O.; Hanfland, M.; Fitch, A. N.; Häuserman, D. *High Pressure Res.* **1996**, *14*, 235−248.
(10) Louër, D.; Louër, M. *J. Appl. Crystallogr.* **1972**, *5*, 271−275.
(11) Altomare, A.; Burla, M. C.; Camalli, M.; Carrozzini, B.; Cascarano, G. L.; Giacovazzo, G.; Guagliardi, A.; Moliterni, A. G. G.; Polidori, G.; Rizzi, R. *J. Appl. Crystallogr.* **1999**, *32*, 339−340.
(12) Larson, A. C.; von Dreele, R. B. *GSAS*; Los Alamos National Laboratory Report LAUR 86-748 (*GSAS*, version June 2001); Los Alamos National Laboratory: Albuquerque, NM, 1985−2002.
(13) Damen, T. C.; Proto, S. P. S.; Tell, B. *Phys. Rev.* **1966**, *142*, 570−574.
(14) Otto, J. W.; Vassiliou, J. K.; Frommeyer, G. *Phys. Rev. B* **1998**, *57*, 3253−3263.
(15) Payne, M. C.; Teter, M. P.; Allan, D. C.; Arias, T. A.; Joannopoulos, J. D. *Rev. Mod. Phys.* **1992**, *64*, 1045−1097.
(16) Kresse, G.; Joubert, D. *Phys. Rev.* **1999**, *B59*, 1758−1775.
(17) Perdew, J. P.; Burke, K.; Ernzerhof, M. *Phys. Rev. Lett.* **1996**, *77*, 3865−3868.

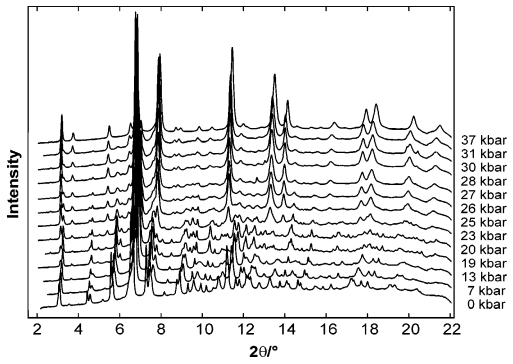

Figure 3. Pressure-dependent X-ray diffraction patterns of $Cs_2[PdI_4]\cdot I_2$ and $Cs_2[PdI_6]$ collected at ID09 of the ESRF (averaged full-width at half-maximum: 0.041° at 7 kbar and 0.055° at 37 kbar).

electrons, are convenient for the study of electronic structures at high pressure. All calculations were controlled for convergence with respect to *k*-point sampling. A 6 × 6 × 6 Monkhurst−Pack scheme was found to be sufficiently accurate for the investigated systems.

3. Results and Discussion

3.1. $Cs_2[PdI_4]\cdot I_2$ to $Cs_2[PdI_6]$. Between ambient pressure and 37 kbar, powder X-ray diffraction patterns were collected at 11 different pressures. The pressure-induced changes of the diffraction patterns in the regime of the transition are displayed in Figure 3. Rietveld refinements of the structural models of $Cs_2[PdI_4]\cdot I_2$ (*I*4/*mmm*) and $Cs_2[PdI_6]$ ($Fm\bar{3}m$) using the collected high-pressure X-ray diffraction data (Figure 4) were performed using the computer program GSAS.[12] Above 19 kbar, the tetragonal crystal structure of $Cs_2[PdI_4]\cdot I_2$ distorts and the metric becomes compatible with an orthorhombic lattice. Although results below 27 kbar are obscured by small amounts of remaining $Cs_2[PdI_4]\cdot I_2$ in the phase, a crystal structure model with *Immm* symmetry results in excellent agreement of calculated and experimental intensity data between 19 and 27 kbar. A strong indication for this phase transition is the steep decrease of the mole fraction of $Cs_2[PdI_4]\cdot I_2$ above 19 kbar and the emergence of the orthorhombic phase $Cs_2[PdI_4]\cdot I_2$. However, the onset of the steep decrease of the intermolecular Pd−I(2) distance is observed above 25 kbar and is paralleled by a significant increase of the bond length I(2)−I(2) (Figure 5). The amount of $Cs_2[PdI_4]\cdot I_2$ diminishes continuously and disappears completely after an annealing cycle at 33 kbar to a maximum temperature of 473 K and subsequent cooling to room temperature (cycle duration ca. 60 min). The resulting $Cs_2[PdI_6]$ with $Fm\bar{3}m$ symmetry is monophasic, as determined by powder X-ray diffraction data (Figure 4), and corresponds to the thermodynamically stable modification of the compound at ambient conditions.

Taking into account the findings concerning the volume dependence of the observed crystal structures, the formation of cubic $Cs_2[PdI_6]$ can be deduced from the pressure-induced changes in $Cs_2[PdI_4]\cdot I_2$. The coordination sphere of the embedded iodine dumbbells consists of four planar $[PdI_4]$ units, which are oriented perpendicular to the bond axis of the iodine dumb bell. With decreasing crystal volume, the distance between $[PdI_4]$ units and the iodine molecules

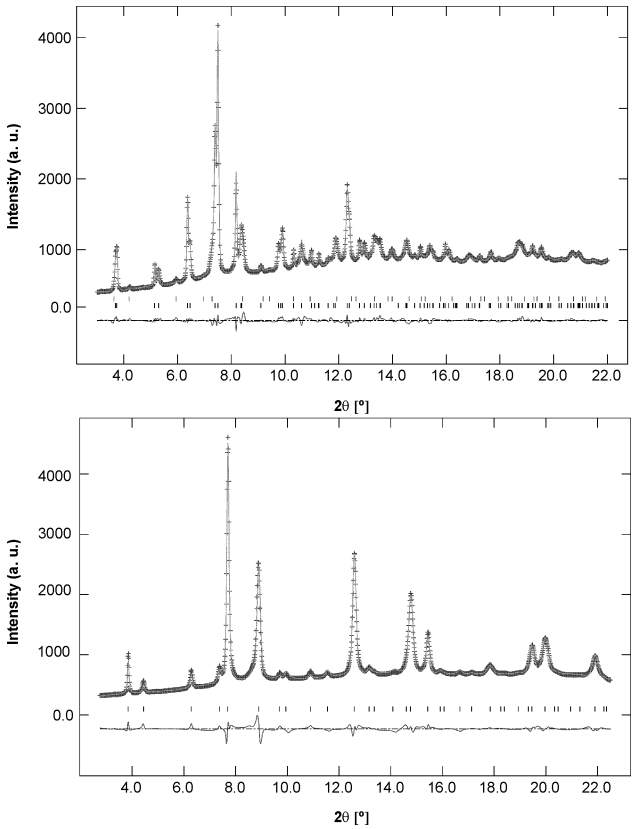

Figure 4. Observed (+) and calculated (−) profiles of the Rietveld refinements of $Cs_2[PdI_4]\cdot I_2$ and $Cs_2[PdI_6]$ at 1 bar (top) and 33 kbar (bottom), respectively. The curves below the diffraction patterns display difference plots, and allowed Bragg positions are represented by tick marks. The second phase in the top diagram is attributed to $Cs_2[PdI_6]$.

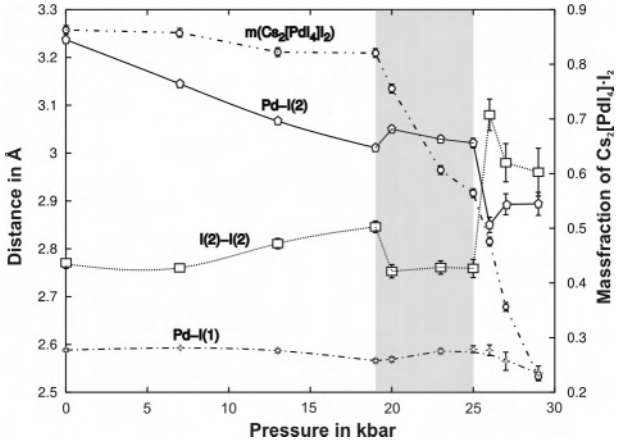

Figure 5. Selected distances at various pressures as extracted from the Rietveld refinements of powder X-ray diffraction data of $Cs_2[PdI_4]\cdot I_2$ and $Cs_2[PdI_6]$. The lines are only a guide to the eyes.

dramatically reduces and intermolecular interactions between these species are enhanced significantly. Simultaneously, the intramolecular iodine distances I(2)−I(2) increase. Finally, the I_2 bonds break and new bonds between iodine and palladium are formed, resulting in cubic $Cs_2[PdI_6]$ with octahedral $[PdI_6]$ units and palladium in the oxidation state 4+.

3.2. $Cs_2[PdBr_4]\cdot I_2$ to $Cs_2[PdBr_4I_2]$. The compound $Cs_2[PdBr_4]\cdot I_2$ (see Table 1) is isostructural to $Cs_2[PdI_4]\cdot I_2$ at ambient pressure. However, the point symmetry of the $[PdBr_4]\cdot I_2$ fragments can maximally retain a D_{4h} symmetry

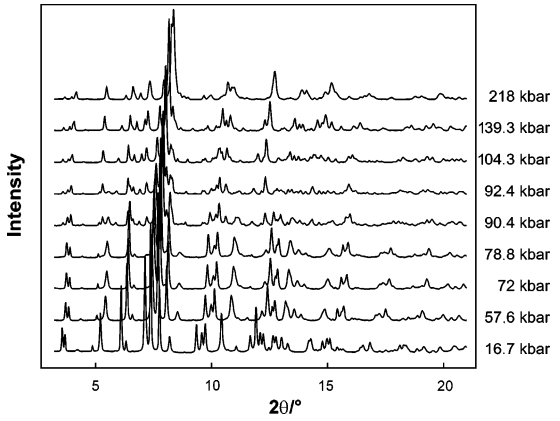

Figure 6. Pressure-dependent powder X-ray diffraction patterns of $Cs_2[PdBr_4]\cdot I_2$ and $Cs_2[PdBr_4I_2]$ collected at ID30 of the ESRF (averaged full-width at half-maximum: 0.038° at 16.7 kbar and 0.085° at 218 kbar).

Table 1. Comparison of Calculated (0 K) and Experimental (in Parentheses) Lattice Parameters and Atomic Positions at Ambient Conditions

compound	*a* [Å]	*c* [Å]	fractional coordinates
$Cs_2[PdBr_4]\cdot I_2$	8.2448 (8.489)	8.7498 (9.085)	Br (8h), $x = 0.7919$ (0.7919) I (4c), $z = 0.6616$ (0.6518)

when transformed to $[PdBr_4I_2]$ while $[PdI_4]I_2$ fragments (D_{4h}) may change to O_h symmetry in $[PdI_6]$ units.

Between ambient pressure and 218 kbar, 22 powder diffraction patterns were collected. In the regime between 1 bar and 78 kbar, the diffraction patterns only shift toward higher diffraction angles upon increasing pressure, which is consistent with earlier results.[18] Around 90 kbar (Figure 6), a new phase emerges that exhibits additional reflections and peak splitting. Indexing on the basis of 12 reflections revealed a monoclinic solution, yielding a figure of merit M(12) = 28.[19] Using this unit cell, the diffraction pattern of the high-pressure modification (number of calculated reflections 317; number of resolved observations 57) could be indexed completely by employing standard computer programs.[10,11] On the basis of this result, a model with the highest diffraction symmetry *C*2/*m* using a nonconventional unit cell setting *I*2/*m* was chosen as a test model (see Tables 2 and 3). In the measured 2θ range, intensities were extracted by the Le Bail method, and all atoms could be allocated in the unit cell by direct methods. In the pressure range between 90 and 104 kbar, both the tetragonal and monoclinic phases coexist. Above 104 kbar, only reflections of monoclinic $Cs_2[PdBr_4I_2]$ were observed in the diffraction patterns. Up to the highest investigated pressure of 218 kbar, the monoclinic phase remained stable.

After the pressure was released, a powder diffraction pattern of the original phase with strongly broadened diffraction peaks was retained. The pressure-dependent changes in the X-ray diffraction patterns are displayed in Figure 6.

(18) Heines, P.; Keller, H.-L.; Bouvier, P.; Hanfland, M. *Z. Anorg. Allg. Chem.* **2003**, *629*, 545−550.
(19) de Wolff, P. M. *J. Appl. Crystallogr.* **1968**, *1*, 108−113.

Table 2. Details of the High-Pressure Rietveld Refinement of $Cs_2[PdBr_4]\cdot I_2$ at 90.5(1) kbar[a]

pressure [kbar]	90.5(1)
cryst syst	monoclinic
space group	*I*2/*m* (No. 12)
a [Å]	8.089(2)
b [Å]	7.319(2)
c [Å]	8.297(2)
β [deg]	93.012(1)
V [Å^3]	490.5(2)
λ [Å]	0.3738
no. of data	1534
no. of obsd reflns	494 (3rd-phase N_2)
no. of param	58
R_p/wR_P	1.18/1.15
R_F^2/χ^2	13.7/0.55

[a] Standard deviations of the last significant digit are given in parentheses.

Table 3. Fractional Coordinates for $Cs_2[PdBr_4]\cdot I_2$ at 90.5(1) kbar (U_{iso} Fixed)[a]

atom	*x*	*y*	*z*	U_{iso} [Å^2]
Pd	0	0	0	0.02
Cs	0.527(1)	0	0.248(2)	0.02
Br	0.797(2)	0.231(2)	0.980(1)	0.02
I	0.976(2)	0	0.323(1)	0.02

[a] Standard deviations are given in parentheses.

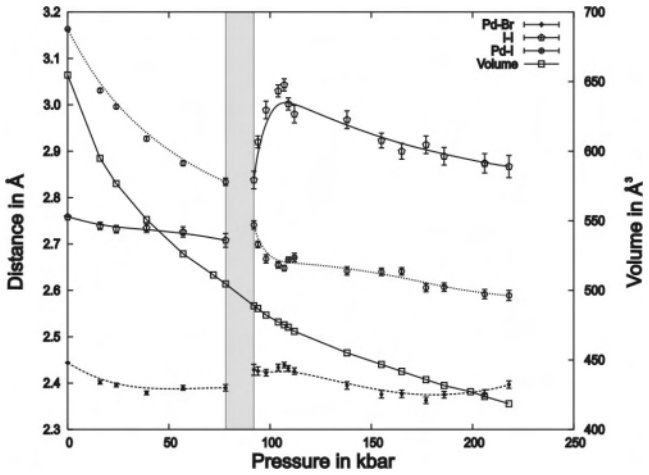

Figure 7. Selected distances calculated from Rietveld refinements of powder X-ray diffraction data of $Cs_2[PdBr_4]\cdot I_2$ and $Cs_2[PdBr_4I_2]$. The lines are only a guide to the eyes.

Changes of interatomic distances as revealed by Rietveld refinements are most pronounced between 78 and 90 kbar, where the intramolecular distance within the I_2 molecule increases dramatically while the I−Pd distance decreases markedly. This is the same pressure region where clear changes in the high-pressure Raman scattering data indicate changes in the local symmetry (see below). With respect to metrical changes, starting at 104 kbar and continuing above this transition region, a quasi-linear relationship of the unit cell parameters, the monoclinic angle, and the interatomic distances is observed with rising pressures (see Figures 7 and 8).

The finding of a structural transition using X-ray diffraction is supported by high-pressure Raman experiments. To make a full symmetry assignment to the observed Raman modes for the low-pressure phase, a factor group analysis was performed. $Cs_2[PdBr_4]\cdot I_2$ has nine atoms in the corre-

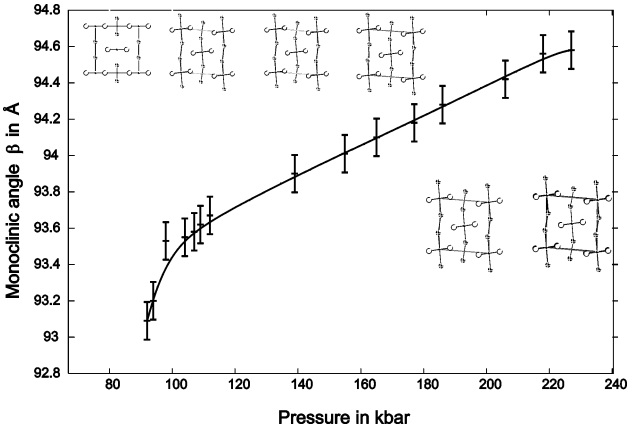

Figure 8. Monoclinic angle β of $Cs_2[PdBr_4]\cdot I_2$ and $Cs_2[PdBr_4I_2]$ at various pressures. The line is only a guide to the eyes.

Table 4. Vibrational Modes of the Compound $Cs_2[PdBr_4]\cdot I_2$

atom	Wyckoff position	point symmetry	irreducible representations
Pd	2a	D_{4h}	$A_{2u} + E_u$
Cs	4d	D_{2d}	$A_{2u} + B_{1g} + E_g + E_u$
I	4e	C_{4v}	$A_{1g} + A_{2u} + E_g + E_u$
Br	8h	C'_2v	$A_{1g} + A_{2g} + A_{2u} + B_{1g} + B_{1u} + B_{2g} + E_g + 2E_u$

sponding primitive unit cell, which give raise to 27 vibrations at $k = 0$ ($\Gamma = 2A_{1g} + A_{2g} + 4A_{2u} + 2B_{1g} + B_{1u} + B_{2g} + 3E_g + 5E_u$).[20] Of these vibrations, eight modes are Raman-active,[21] i.e., two A_{1g}, two B_{1g}, one B_{2g}, and three E_g. Table 4 lists the modes for each atomic position.

As can be seen from the results of the analysis (Table 4), it is not sufficient to perform only a symmetry assignment of the observed modes to detect the A_{1g} (stretching) and E_g (bending) modes, which in the first approximation are mainly determined by the force constant of the I−I bond.

To clarify the question of which of the A_{1g} and E_g modes can be attributed to the I_2 unit, additional oriented and polarized experiments with single crystals were conducted using the isostructural compound $Rb_2[PdBr_4]\cdot I_2$.[18] The corresponding modes are expected to exhibit similar frequencies because the I−I distances in both compounds are nearly identical [Cs, 2.759(1) Å; Rb, 2.755(4) Å]. Under the assumption of similar force constants in analogous compounds, the spectra obtained from single crystals (Figure 9) result in the finding that the intense modes at 158 cm^{-1} (A_{1g}) and 160 cm^{-1} (E_g) can be attributed to the I−I interaction in the compounds $Rb_2[PdBr_4]\cdot I_2$ and $Cs_2[PdBr_4]\cdot I_2$ at ambient pressure. The lower vibrational frequency observed, compared to I_2 in the gas phase at 213.34 cm^{-1},[22] is due to the weaker I−I bonding, as indicated by the longer I−I distance (2.77 Å instead of 2.66 Å).[23] Selected Raman spectra of $Cs_2[PdBr_4]\cdot I_2$ and $Cs_2[PdBr_4I_2]$ obtained at high pressures are depicted in Figure 10.

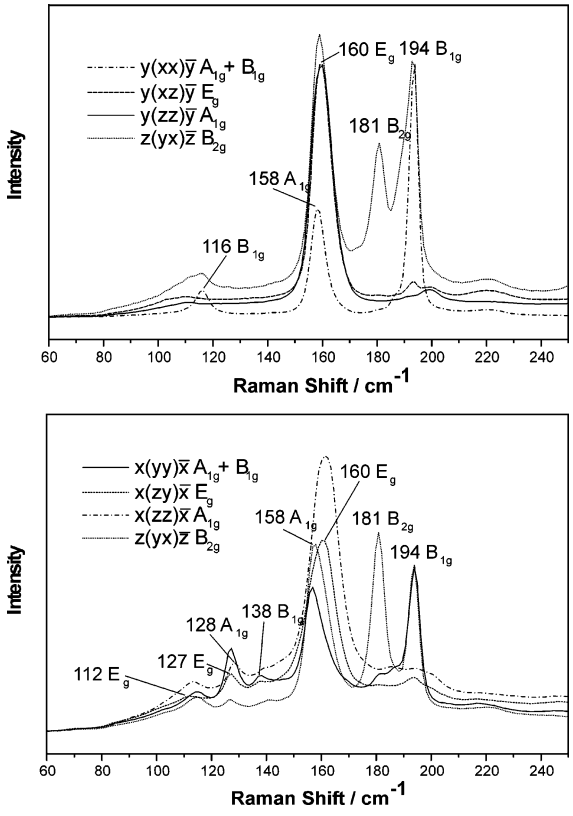

Figure 9. Polarized Raman spectra of $Cs_2[PdBr_4]\cdot I_2$ and $Rb_2[PdBr_4]\cdot I_2$.

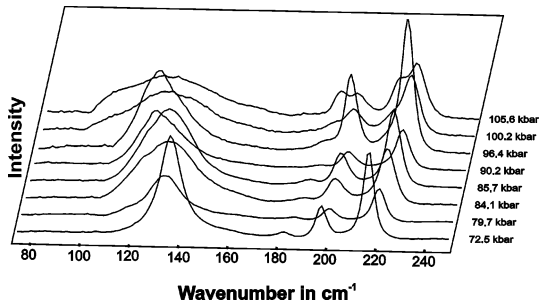

Figure 10. High-pressure Raman measurements of $Cs_2[PdBr_4]\cdot I_2$ and $Cs_2[PdBr_4I_2]$.

With increasing pressure, the corresponding I−I modes shift to lower frequencies and become very broad. The slope change between 90 and 95 kbar in the shift of the modes is taken as an indicator of a successive weakening in the I−I interaction (Figure 11). In contrast, the frequencies of the other modes observed increase with rising pressure. Associated with the structural changes are two effects influencing the vibrational frequencies: (i) a change in the oxidation state of the central atom from 2+ to 4+ and (ii) an increase of the coordination number of Pd from 4 to 6. While the first effect should result in higher frequencies of the Pd−Br vibrations, the second effect shifts the modes toward lower frequencies again.[21] The increasing frequencies in the experiment not only reflect the stronger effect caused by the oxidation state change but also evidence the ongoing redox reaction. In accordance with the symmetry reduction, resolved by X-ray diffraction, an additional splitting of the modes at approximately 200 cm^{-1} is seen by Raman scattering.

(20) Rousseau, D. L.; Bauman, R. P.; Proto, S. P. S. *J. Raman Spectrosc.* **1981**, *10*, 253−290.
(21) Weidlein, J.; Müller, U.; Dehnicke, K. *Schwingungsspektroskopie*; Thieme: Stuttgart, Germany, 1988.
(22) Stammreich, H.; Forneris, R.; Tavares, Y. *Spectrochim. Acta* **1961**, *17*, 1173−1184.
(23) Pauling, L. *The nature of the chemical bond*, 3rd ed.; Cornell University Press: Ithaca, NY, 1960.

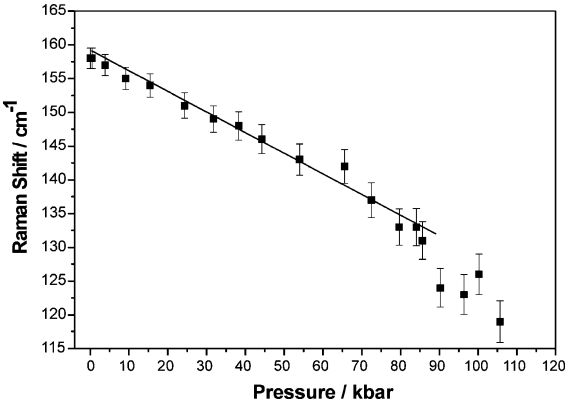

Figure 11. Pressure-dependent shift of the A_{1g} mode of $Cs_2[PdBr_4]\cdot I_2$ and $Cs_2[PdBr_4I_2]$. The straight line is a guide to the eyes.

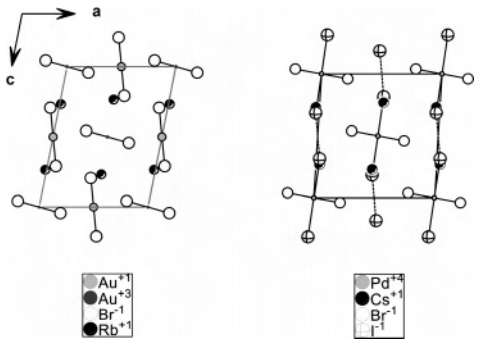

Figure 12. Relationship between the crystal structures of $Rb_2[AuBr_4]$-$[AuBr_2]$ and $Cs_2[PdBr_4I_2]$.

Thus, analogous to $Cs_2[PdI_4]\cdot I_2$, the experimental findings are consistent with an internal redox reaction of the compound $Cs_2[PdBr_4]\cdot I_2$ at pressures between 78 and 104 kbar. Here, the intramolecular I_2 bonds are cleaved and new Pd−I bonds are formed.

The high-pressure crystal structure of $Cs_2[PdBr_4I_2]$ is closely related to that of $Rb_2[AuBr_4][AuBr_2]$,[24] which comprises a monoclinically distorted crystal structure motif of the $Cs_2Au_2Cl_6$ type (Figure 12). The structure of Cs_2-$[PdBr_4I_2]$ consists of distorted octahedral $[PdBr_4I_2]$ units with palladium in the oxidation state 4+. Each palladium is surrounded by four equidistant bromide ions. The palladium coordination is extended by two iodide ions on top of these square-planar units to form slightly distorted octahedral $[PdBr_4I_2]$ units. The distances between palladium and iodine are significantly shorter (ca. 0.3−0.4 Å) than the distances between adjacent iodine atoms and are located well within the bond range found for Pd^{4+}. Every $[PdBr_4I_2]$ unit is coordinated by eight cesium atoms in the form of a highly distorted cube. Crystallographic details for $Cs_2[PdBr_4I_2]$ at 90 kbar are shown in Tables 2 and 3.

The results of the theoretical calculations can be visualized by the equation of state (EOS) for tetragonal $Cs_2[PdBr_4]\cdot I_2$ (*I*4/*mmm*) and monoclinic $Cs_2[PdBr_4I_2]$ (*I*2/*m*) crystal structures (Figure 13). By the common tangent method to the EOS[25] of each phase, the tetragonal to monoclinic transformation pressure was determined to be 73 kbar and is in good agreement with the values derived from X-ray diffraction (78−104 kbar) and Raman scattering (90−95 kbar). A comparison of calculated and observed structural parameters is given in Table 5. The agreement between theory and experiment is excellent. The calculations substantiate the experimental observation that the phase transition results in the breaking of the I−I bond in the I_2 moiety, resulting in the formation of $[PdBr_4I_2]$ octahedra. As is visible in the EOS of the two phases, the energy for the monoclinic modification is very competitive with that of the tetragonal phase at volumes that correspond to pressures in the 55−80 kbar region. This is consistent with the experimental finding that these two phases coexist at high pressure.

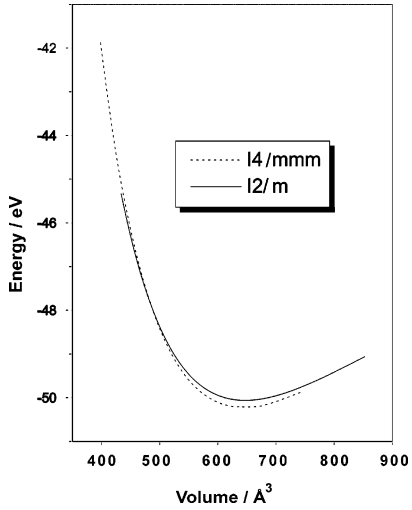

Figure 13. Energy vs volume calculation for $Cs_2[PdBr_4]\cdot I_2$.

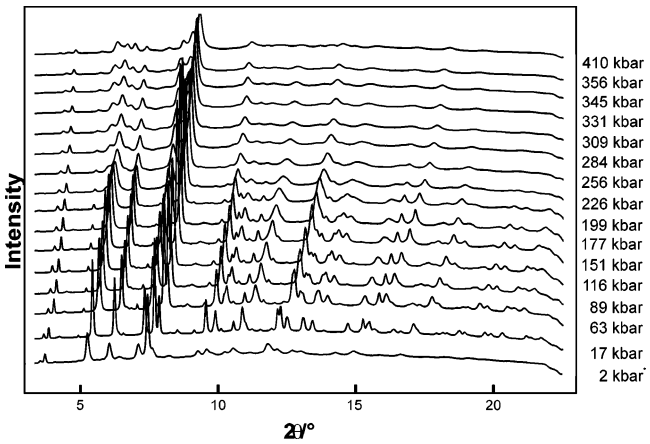

Figure 14. Pressure-dependent X-ray diffraction patterns of $Cs_2[PdCl_4]\cdot I_2$ and $Cs_2[PdCl_4I_2]$ collected at ID30 of the ESRF (averaged full-width at half-maximum: 0.042° at 17 kbar and 0.097° at 256 kbar). The asterisk indicates the 2 kbar line after pressure release.

3.3. $Cs_2[PdCl_4]\cdot I_2$ to $Cs_2[PdCl_4I_2]$. Similar to $Cs_2[PdBr_4]\cdot I_2$, the compound $Cs_2[PdCl_4]\cdot I_2$ can maximally retain D_{4h} symmetry when the transformation from $Cs_2[PdCl_4]\cdot I_2$ into $Cs_2[PdCl_4I_2]$ takes place. Because of the smaller distance between the central atom and halide ligands and the increased bond strength, the approach of the iodine molecule is sterically hindered and, thus, the transition pressure of palladium from 2+ to 4+ is expected to be higher compared to $Cs_2[PdBr_4]\cdot I_2$. Two series of powder X-ray diffraction

(24) Strähle, J.; Gelinek, J.; Kölmel, Z. *Z. Anorg. Allg. Chem.* **1979**, *456*, 241−260.
(25) Yin, M. T.; Cohen, M. L. *Phys. Rev. Lett.* **1983**, *50*, 2006−2009.

Table 5. Comparison of Calculated and Experimental Values for the Crystal Structures of $Cs_2[PdBr_4]\cdot I_2$ and $Cs_2[PdBr_4I_2]$ at Selected Pressures (Experimental Values in Parentheses)

		$Cs_2[PdBr_4]\cdot I_2$ (*I*4/*mmm*) for $p = 40$ kbar (39 kbar)			
a [Å]	8.0907 (8.0087)	Pd	0 (0)	0 (0)	0 (0)
		Cs	3/4 ($^3/_4$)	$^1/_4$ ($^1/_4$)	$^1/_2$ ($^1/_2$)
c [Å]	8.6836 (8.5890)	Br	0.2153 (0.2401)	0.2153 (0.2401)	0.4306 (0.4802)
		I	0.3330 (0.3408)	0.3330 (0.3408)	0 (0)
		$Cs_2[PdBr_4]\cdot I_2$ (*I*4/*mmm*) for $p = 75$ kbar (72 kbar)			
a [Å]	7.7901 (7.7983)	Pd	0 (0)	0 (0)	0 (0)
		Cs	$^3/_4$ ($^3/_4$)	$^1/_4$ ($^1/_4$)	$^1/_2$ ($^1/_2$)
c [Å]	8.5365 (8.4040)	Br	0.2234 (0.2183)	0.2234 (0.2181)	0.4469 (0.4396)
		I	0.3209 (0.3359)	0.3209 (0.3359)	0 (0)
		$Cs_2[PdBr_4I_2]$ (*I*2/*m*) for $p = 90$ kbar (90 kbar)			
a [Å]	8.3992 (8.2928)	Pd	0 (0)	0 (0)	0 (0)
b [Å]	7.3097 (7.3289)	Cs	0.7306 (0.7512)	$^1/_2$ ($^1/_2$)	0.0323 (0.0274)
c [Å]	8.1918 (8.0863)	Br	0.0320 (0.0135)	0.7627 (0.7632)	0.7867 (0.7862)
β [deg]	93.56 (93.05)	I	0.6811 (0.6735)	0 (0)	0.0226 (0.0228)
		$Cs_2[PdBr_4I_2]$ for (*I*2/*m*) for $p = 112$ kbar (113 kbar)			
a [Å]	8.3258 (8.2726)	Pd	0 (0)	0 (0)	0 (0)
b [Å]	7.1669 (7.0993)	Cs	0.7280 (0.7656)	$^1/_2$ ($^1/_2$)	0.0345 (0.0355)
c [Å]	8.1249 (8.0290)	Br	0.0353 (0.0388)	0.7585 (0.7630)	0.7858 (0.7830)
β [deg]	93.71 (93.67)	I	0.6830 (0.6399)	0 (0)	0.0265 (0.0270)

experiments were recorded between ambient pressure and 410 kbar at a total of 40 different pressures. Between ambient pressure and 256 kbar, the structural model of $Cs_2[PdCl_4]\cdot I_2$ was refined by least-squares procedures using full diffraction profiles and applying Rietveld's method. Above 256 kbar, the reflection peaks broaden too much or exhibit splitting and prohibit a reliable profile refinement.

Consequently, no satisfactory crystal structure refinement above this point could be achieved. The results show that below 177 kbar the relationship between lattice parameters and pressure can be described as linear. After pressure release, a powder diffraction pattern of $Cs_2[PdCl_4]\cdot I_2$ with significantly broadened reflections is retained (Figure 14).

Within the stability range of the low-pressure phase, the atomic distances as derived by the Rietveld refinements indicate expanding Pd−Cl distances within the $[PdCl_4]$ units (Figure 15), which is typical for an increase in the coordination number, such as in a $[PdCl_4I_2]$ unit. This expansion of the [4 + 2] coordination coincides with the decreasing Pd−I distance. Above 170 kbar, the I−I distances increase rapidly, whereas the Pd−I and Pd−Cl distances decrease, as indicated by the crystal structure data (Figure 15 and Tables 6 and 7). Thus, the observed pressure-induced structural changes of $Cs_2[PdCl_4]\cdot I_2$ are in accordance with the onset of a solid-state redox reaction to $Cs_2[PdCl_4I_2]$ in the range between 120 and 160 kbar.

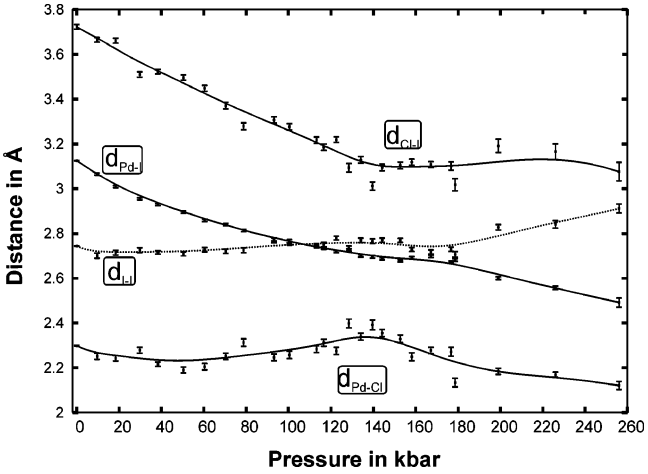

Figure 15. Selected interatomic distances calculated from Rietveld refinements of powder X-ray diffraction data of $Cs_2[PdCl_4]\cdot I_2$ and $Cs_2[PdCl_4I_2]$. The lines are a guide to the eyes.

Table 6. Details of the High-Pressure Rietveld Refinement of $Cs_2[PdCl_4]\cdot I_2$ at 139.2(1) kbar[a]

pressure [kbar]	139.2(1)
cryst syst	tetragonal
space group	*I*4/*mmm* (No. 139)
a [Å]	7.2537(3)
c [Å]	8.1572(4)
V [Å^3]	429.21(3)
λ [Å]	0.3738
no. of data points	1489
no. of obsd reflns	121 (2nd-phase N_2)
no. of param	30
R_p/wR_p	2.68/4.15
R_F^2/χ^2	9.96/0.75

[a] Standard deviations are given in parentheses.

Table 7. Fractional Coordinates for $Cs_2[PdCl_4I_2]$ at 140 kbar[a]

atom	*x*	*y*	*z*	U_{iso} [Å^2]
Pd	0	0	0	0.033(2)
Cs	0	$^1/_2$	$^1/_4$	0.026(2)
Br	0.233(2)	0.233(2)	0	0.060(6)
I	0	0	0.3304(6)	0.012(1)

[a] Standard deviations are given in parentheses.

4. Conclusions

An investigation of a solid-state redox reaction with an associated structural phase transition of $Cs_2[PdI_4]\cdot I_2$ to $Cs_2[PdI_6]$ has been performed using high-pressure synchrotron powder X-ray diffraction experiments. Taking into account that in the tetragonal crystal structure the crystallographic *c* axis and, thus, the direction of the approaching I_2 molecules are parallel to the *z* direction of the square-planar palladium complexes, the $Cs_2[PdI_4]\cdot I_2$ to $Cs_2[PdI_6]$ transition is driven by increasing interactions between palladium d_{z^2} orbitals and the iodine molecular orbitals. The elongation of the intramolecular bonds within the iodine dumbbells is supported by

the pressure of the neighboring iodine atoms on this bond. However, on the basis of the presented experiments, we cannot extract whether the final step of the redox reaction is a one- or two-step mechanism.

The crystal structures of the high-pressure phases of $Cs_2[PdBr_4]\cdot I_2$ and $Cs_2[PdCl_4]\cdot I_2$ have been determined by full-profile refinements of synchrotron powder X-ray diffraction data. In contrast to the system $Cs_2[PdI_4]\cdot I_2/Cs_2[PdI_6]$ with a potentially cubic high-pressure phase, the resulting $[Pd^{4+}X_4I_2]$ complexes (X = Br, Cl) can maximally retain D_{4h} symmetry. However, the high-pressure modification of $Cs_2[PdBr_4]\cdot I_2$ adopts a significantly lower symmetry. The results of the diffraction experiments clearly indicate that $Cs_2[PdBr_4I_2]$ is the stable species above 104 kbar and that for $Cs_2[PdCl_4I_2]$ the onset of the redox reaction is located between 120 and 160 kbar. The results of the Raman experiments are consistent with the transition pressures determined by the powder X-ray diffraction data for $Cs_2[PdBr_4I_2]$ and the finding that a pronounced decrease of symmetry occurs at the structural phase transition. Both high-pressure modifications $Cs_2[PdX_4I_2]$ (X = Br, Cl) are more stable at elevated pressures than the $Cs_2[PdX_4]\cdot I_2$ low-pressure phases. Upon pressure release, the redox reactions are reversed, and the initial compounds $Cs_2[PdX_4]\cdot I_2$ (X = Br, Cl) are recovered. The experimental results for $Cs_2[PdBr_4]\cdot I_2$ are in excellent agreement with the theoretically calculated EOSs for both the low- and high-pressure phases. Moreover, the electron-transfer mechanism of this type of redox reaction will be the subject of a forthcoming investigation using high-pressure Mössbauer and electron spin resonance spectroscopy.

Acknowledgment. We are indebted to the ESRF for granting the experiments (Grants CH1052 and CH1086) and to the beamline scientists M. Hanfland (ID09) and P. Bouvier (ID30).

Supporting Information Available: Selected crystallographic files in CIF format for $Cs_2[PdI_6]$, $Cs_2[PdBr_4I_2]$, and $Cs_2[PdCl_4I_2]$. This material is available free of charge via the Internet at http://pubs.acs.org.

IC0601945